SHOCK COMPRESSION AND RELEASE IN HIGH-STRENGTH CERAMICS

CONF-890812--6
SAND--89-0918C
DE89 016418

Marlin E. KIPP and Dennis E. GRADY

Sandia National Laboratories, Computational Physics & Mechanics and Thermomechanical & Physical Divisions
Albuquerque, New Mexico 87185-5800 *

Shock compression and release particle velocity data have been obtained for silicon carbide, titanium diboride, boron carbide, and zirconium dioxide with a laser velocity interferometer (VISAR). Peak impact stresses in these experiments range between 20 and 50 GPa. Iterative numerical methods were used to obtain dynamic compression and release stress-strain behavior of the ceramics.

1. INTRODUCTION

Ceramics have been repeatedly demonstrated to be effective armor materials against a variety of threats (*e.g.* Wilkins, *et al.*[1]). Although quasistatic characterization of ceramics is fairly extensive, there are major gaps in the data required for dynamic characterization of these materials. The most complete collection of Hugoniot data has been assembled by Gust and Royce[2] and Gust, *et al.*[3], including Hugoniot elastic limits (HEL) and shock Hugoniots for about a dozen ceramic materials. Further shock wave data is available for a variety of grades of aluminum oxide[4–8], titanium diboride[9], and zirconia[10,11]. Wave profile data in compression and release in uniaxial strain are presented here for B_4C, SiC, TiB_2, and ZrO_2. Additional details may be found in Kipp and Grady[12]. Diverging wave data are currently being generated that focus on the time-resolved particle motion on the back surface of ceramic targets impacted by 2 mm diameter projectiles[13].

2. MATERIALS

Ultrasonic longitudinal, C_L, and shear, C_S, wave speeds, and reference density, ρ_0, were determined for all the ceramic specimens in this study. A summary of these experimental values, accompanied by calculated values for bulk wave speed, C_0, and Poisson ratio, ν, is provided in Table 1.

Table 1: Elastic Properties

Material	ρ_0 kg/m^3	C_L km/s	C_S km/s	C_0 km/s	ν
B_4C	2516	14.04	8.90	9.57	0.164
SiC	3177	12.06	7.67	8.19	0.160
TiB_2	4452	10.93	7.30	6.96	0.097
ZrO_2	5602	6.61	3.54	5.19	0.299

The partially stabilized zirconia (PSZ) contains 12.5 mol % yttria-doped zirconia, and has a porosity of 0.04%. The titanium diboride was determined to be about 1% porous, and the silicon carbide was also found to be about 1% porous. Optical microscopy revealed fine grain equiaxial grain structures for all samples, with nominal grain sizes of 7 μm, 12 μm, 10 μm, and 15 μm for the SiC, TiB_2, B_4C, and ZrO_2, respectively.

3. EXPERIMENTS

Uniaxial strain compressive shock and release waves were produced in the ceramics of interest with a single stage powder gun (89 mm bore diameter, 2.2 km/s maximum impact velocity). The ceramic carried by the projectile was backed by foam, and the target consisted of a disc of similar ceramic backed by an optical quality single crystal of lithium fluoride. The history of the compression and release wave formed by this impact configuration is measured by monitoring the time-resolved longitudinal motion of the ceramic-lithium fluoride interface

*This work performed at Sandia National Laboratories supported by the U.S. DOE under contract #DE-AC04-76DP00789, and funded by the Balanced Technology Initiative through both the Defense Advanced Research Projects Administration and the Army Research Office.

---

using laser velocity interferometry (VISAR) techniques[14] (resolution ~ 1 ns). Two experiments were performed on each of the four materials investigated. The impact velocity and experimental dimensions for each test are provided in Table 2 and the acquired time-resolved velocity profiles are displayed in Figure 1 (low amplitude) and Figure 2 (high amplitude). (The arrival times of the wave profiles were offset to display the records.)

Table 2: Conditions for Ceramic Impact Experiments

Material	Impact Velocity (km/s)	Foam Density (kg/m^3)	Impactor Thickness (mm)	Target Thickness (mm)
B_4C	1.546	320	3.920	9.044
B_4C	2.210	640	3.917	9.033
SiC	1.542	320	3.987	8.939
SiC	2.100	640	3.995	8.940
TiB_2	1.515	320	3.972	10.804
TiB_2	2.113	640	3.337	10.747
ZrO_2	1.556	320	3.313	6.635
ZrO_2	2.075	640	3.247	6.324

4. COMPRESSION AND RELEASE PROPERTIES

The wave profiles shown in Figures 1 and 2 are distorted somewhat in both amplitude and shape due to the mechanical impedance difference between the lithium fluoride and ceramic. Additional insight into the ceramic response to shock loading is gained by transforming the particle velocity history for each experiment into a stress-strain load-release curve. In this way, features in the measured wave profiles associated with wave interactions caused by the sample and window material impedance mismatch can be separated from material response properties of the ceramics (yield, phase transformations, *etc.*). An understanding of the material response interior to the target ceramic also provides a means for determining more clearly the elements necessary to model these materials. In all cases, the analysis was accomplished using the one-dimensional explicit Lagrangian shock wave propagation code, WONDY[15].

Standard material models (*e.g.* elastic-perfectly plastic, strain-hardening plasticity) using ultrasonic reference values (Table 1) and Hugoniot data[2,3] were initially used for each material. Of the four ceramics, only SiC

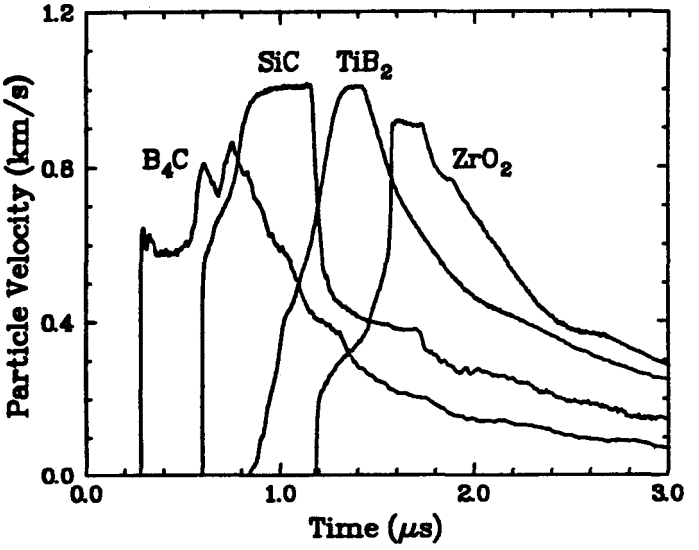

FIGURE 1
Particle velocity data for the four ceramics at the lower impact velocity.

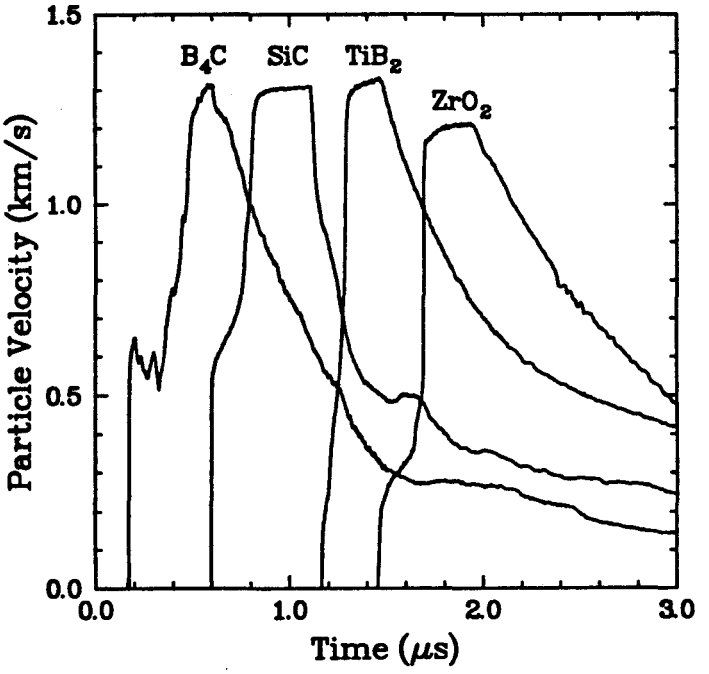

FIGURE 2
Particle velocity data for the four ceramics at the higher impact velocity.

could be readily represented with a traditional strain-hardening model which captured nearly all of its load and release response (indicating full retention of yield strength.) For the other three ceramics in this study, the limitations of the elastic-perfectly plastic assump-

tions were to be found primarily in the inability to accommodate the very dispersive nature of the unloading wave.

To obtain accurate internal stress-strain histories, a technique patterned after that developed by Grady and Furnish[16] was used, in which a parametrized load-unload path was incorporated into WONDY, and exercised in an iterative fashion. Spline-fit points defined loading and unloading paths that were adjusted for each ceramic experiment until the VISAR interface particle velocity history was reproduced. We have assumed that the primary contribution to the stress is the material strain, and dependence on both strain rate or thermal effects has been neglected. Ultrasonic data were used to define the initial loading moduli.

Load-release paths for the four ceramics are compared in Figures 3 (low amplitude) and 4 (high amplitude). These paths are taken at the center of the target ceramic. Note that although there is almost a factor of two spread in densities, the elastic loading curves of B_4C, SiC, and TiB_2 are very nearly identical in both low and high amplitude cases. The B_4C shows a major loss in strength when compared to the other two ceramics. Although the SiC and TiB_2 respond similarly in the low amplitude impact, at the higher impact velocities, the TiB_2 is stiffer than either of the other two, with the B_4C still being the weakest of these three. ZrO_2 undergoes the largest strains at these impact velocities.

The Hugoniot elastic limits for the various ceramics tested were determined directly from the measured particle velocity profiles (Figures 1-2) accounting for the impedance mismatch between ceramic and window. The expression used was $\sigma_{HEL} = \frac{Z_C+Z_L}{2} u_M$ where Z_C and Z_L are the appropriate shock impedances for the ceramic and lithium fluoride, respectively, and u_M is the observed particle velocity amplitude selected from each profile which represents the transition from elastic to nonelastic behavior. For the ceramic, $Z_C = \rho_0 C_L$, since within experimental uncertainty, the finite amplitude elastic velocities and ultrasonic velocities were the same. For lithium fluoride $Z_L = \rho_0(C_0 + s u_M)$ with ρ_0 = 2641 kg/m^3, C_0 = 5148 m/s, and s = 1.353.

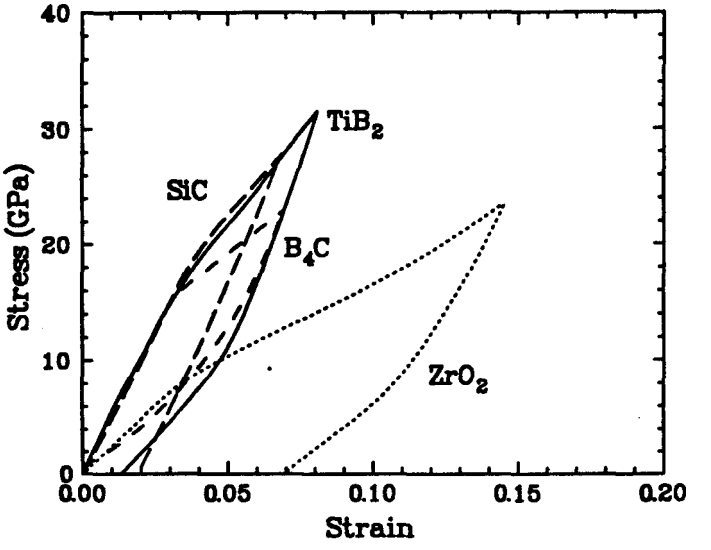

FIGURE 3
Summary of calculated stress-strain load-release paths for the four ceramics at the lower impact velocity.

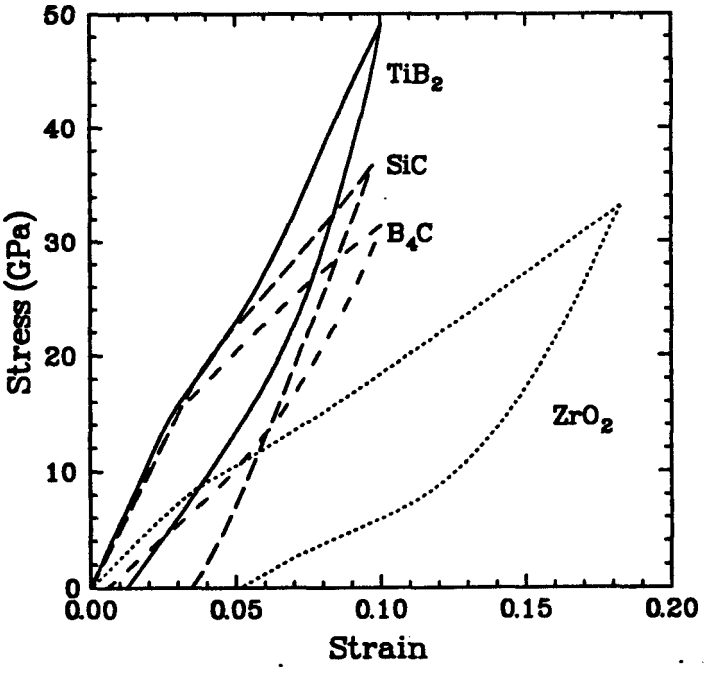

FIGURE 4
Summary of calculated stress-strain load-release paths for the four ceramics at the higher impact velocity.

The Hugoniot elastic limit data (σ_{HEL}) are tabulated in Table 3. For silicon carbide the initial break from the steeply rising initial wave to the ramping region above this wave was chosen for u_M. For boron carbide u_M was determined from the somewhat noisy plateau re-

gion between the first and second wave. (This noise is thought to reflect heterogeneous yielding processes.) The structure of the compressive wave for titanium diboride caused difficulty in unambiguously selecting a particle velocity corresponding to the HEL. A reasonably well-defined break in both waves at approximately 160 m/s was tentatively selected as a preliminary yield process or phase transformation u_M value. There is a second break at about 420 m/s, however, which is also a consequence of some structuring feature in the TiB_2 material response. This is also identified in Table 3. The appropriate u_M for zirconium dioxide was determined from the break between steep and ramped wave behavior. These values of σ_{HEL} are consistent with those determined in the WONDY numerical analysis.

Table 3: Hugoniot Elastic Limits

Test No.	Material	u_M (m/s)	σ_{HEL} (GPa)	P_H (GPa)
1	B_4C	580±30	14.8	22.8
2	B_4C	550±40	14.0	31.4
3	SiC	550±30	14.8	27.6
4	SiC	570±30	15.3	36.5
5	TiB_2	165±15	5.2	31.0
"	"	430±40	13.7*	"
6	TiB_2	150±15	4.7	48.5
"	"	410±20	13.1*	"
7	ZrO_2	195±10	5.0	23.6
8	ZrO_2	210±10	5.4	33.2

* Corresponds to second yield structure in TiB_2

5. CONCLUSIONS

The present set of eight experiments on silicon carbide, boron carbide, titanium diboride, and zirconium dioxide provide an overview of the wide range of possible response of ceramics to dynamic compressive loading and release. The large yield strengths associated with ceramics are verified. The titanium diboride exhibits significant dispersion of compression waves to 50 GPa. The boron carbide, titanium diboride, and zirconium dioxide disperse the release waves more widely than normal solid response should be, suggesting that internal damage during compression has altered the state of the material. Only silicon carbide exhibits traditional elastic-strain hardening-plastic response to shock loading. The continuous load-release curves provide a substantial database for evaluating computational models.

REFERENCES

1. M. L. Wilkins, C. F. Cline, and C. A. Honodel, Lawrence Radiation Laboratory Report UCRL-71817 (1969).
2. W. H. Gust and E. B. Royce, J. Appl. Phys. 42 (1971) 276.
3. W. H. Gust, A. C. Holt, and E. B. Royce, J. Appl. Phys. 44 (1973) 550.
4. T. J. Ahrens, W. H. Gust, and E. B. Royce, J. Appl. Phys. 39 (1968) 4610.
5. J. Cagnoux and F. Longy, J. de Physique, Colloque C3, 49 (1988) 3.
6. D. E. Munson and R. J. Lawrence, J. Appl. Phys. 50 (1979) 6272.
7. Z. Rosenberg, J. Appl. Phys. 57 (1985) 5087.
8. D. Yaziv, Y. Yeshurun, Y. Partom, and Z. Rosenberg, in Shock Waves in Condensed Matter 1987, eds. S. C. Schmidt, N. C. Holmes, (Elsevier, 1988), 297.
9. D. Yaziv and N. S. Brar, J. de Physique, Colloque C3, 49 (1988) 683.
10. T. Mashimo, K. Nagayama, and A. Sawaoka, Phys. and Chem. Minerals 9 (1983) 237.
11. T. Mashimo (1988) J. Appl. Phys. 63 (1988) 4747
12. M. E. Kipp and D. E. Grady, Sandia National Laboratories Report SAND89-1461 (1989).
13. J. L. Wise and M. E. Kipp, Time-Resolved Penetration Response of Ceramic and Steel Plates, this volume.
14. L. M. Barker and R. E. Hollenbach, J. Appl. Phys. 43 (1972) 4669.
15. M. E. Kipp and R. J. Lawrence, Sandia National Laboratories Report SAND81-0930 (1982).
16. D. E. Grady and M. D. Furnish, Sandia National Laboratories Report SAND88-1642 (1988).